Mechanical Systems and Signal Processing 118 (2019) 93–107

Contents lists available at ScienceDirect

Mechanical Systems and Signal Processing

journal homepage: www.elsevier.com/locate/ymssp

Adaptive vibration suppression of time-varying structures with enhanced FxLMS algorithm

Wenchao Niu [a], Chengzhe Zou [b], Bin Li [a,*], Wei Wang [a]

[a] School of Aeronautics, Northwestern Polytechnical University, Xi'an, Shaanxi 710072, China
[b] Department of Mechanical and Aerospace Engineering, The Ohio State University, Columbus, OH 43210, USA

ARTICLE INFO

Article history:
Received 27 February 2018
Received in revised form 29 June 2018
Accepted 3 August 2018

Keywords:
Filtered-x least mean square
Bang-bang control
Variable step size
Online identification
Time-varying structures

ABSTRACT

Filtered-x least mean square (FxLMS) control algorithm has been widely used for adaptive noise and vibration control. Yet, classical FxLMS controller is not applicable for time-varying system since the secondary path identified offline cannot reflect the system characteristics in real-time. In order to overcome this challenge, here online modelling of secondary path is realized by existing signals, i.e. no noise injection. In addition, FxLMS is further enhanced with variable step size that is adaptively adjusted via bang-bang controller. The adaptation of step size is aimed to achieve the balance between control efficiency and system stability. To verify the feasibility of proposed control algorithm, numerical and experimental efforts are undertaken for the buffeting suppression of vertical tail which is a typical time-varying system. Both results demonstrate that the proposed method is able to reduce the vibration response effectively for varied structures under harmonic and random excitations, while the classical FxLMS cannot. This performance improvement indicates that the online modeling of secondary path captures the system characteristics accurately and timely. Moreover, compared with the FxLMS controller with fixed step size, the control efficiency of the proposed method is also strengthened. These multiple enhancements of the performance of FxLMS controller reveal that online modeling and variable step size are favorable for adaptive vibration control of time-varying structures.

1. Introduction

Structural vibration should be concerned due to numerous reasons, including but not limited to fatigue-induced structure failure, excessive wearing of machinery, and radiated noise [1–3]. In order to avoid the aforementioned harms, active vibration control has been investigated for a long time and various control algorithms have demonstrated exceptional performance in practice [4–6]. However, these controllers are usually designed under time-invariant assumption and consequently lack adaptation to the variations of structural characteristics, which leads to challenges for the vibration suppression of time-varying structures. In fact, many engineering structures subject to the threats of vibration are not time-invariant, and the vertical tail of aircraft is a good example [7]. For aircrafts under high angle of attack, the turbulent flow emanating from the wing/fuselage flows downstream to impinge upon the vertical tails [8]. This unsteady flow typically contains considerable energy and its spectrum covers the dominant vibration modes of the vertical tails [9]. Therefore the

* Corresponding author.
E-mail address: leebin@nwpu.edu.cn (B. Li).

https://doi.org/10.1016/j.ymssp.2018.08.009
0888-3270/

fluid-induced structural vibration response, referred to as buffeting, is of high magnitude and threatens the safety of aircrafts [9]. Throughout the described fluid-structure interaction process, the vertical tail is coupled with the aerodynamics and thus its structural dynamics are changed by the coupling. In addition, the coupling effect depends on airspeed and angle of attack of the aircraft according to the wind tunnel outcomes in Ref. [10]. As a consequence, this mechanical system turns from time-invariant into time-varying, which requires adaptive control for real-time vibration reduction [11,12].

In terms of adaptive control algorithms, myriad methods have been implemented in vibration suppression [13–16]. Among them, the adaptive filtered-x least mean square (FxLMS) algorithm has wide applications due to its simplicity and robustness [17–20], which motivates us to employ it in the vibration suppression of the vertical tail. The classical FxLMS algorithm illustrated in Fig. 1 is proposed in Ref. [21], which is based on the gradient descent method [21]. In Fig. 1, $x(n)$ is the external disturbance that usually serves as the feedforward reference signal, where n indicates the time sequence; $d(n)$ is the open-loop response of the primary path $P(z)$ under the excitation of $x(n)$; $S(z)$ is the secondary path to generate response $y'(n)$ to cancel $d(n)$; $e(n)$ is the superposition of $d(n)$ and $y'(n)$, i.e. the residual vibration response; $W(z)$ is the finite impulse response (FIR) filter and its coefficients are adaptively updated to control the secondary path $S(z)$ for minimum $e(n)$ in real-time; the coefficient updates are ruled by least mean square (LMS) algorithm whose inputs are filtered reference signal $x'(n)$ and residual response $e(n)$; $x'(n)$ refers to $x(n)$ filtered by the offline-estimated secondary path $\widehat{S}(z)$.

The optimal solution of $\mathbf{W}(n)$ is obtained by minimizing the error signal [21]

$$\mathbf{W}^* = \mathbf{R}^{-1}\mathbf{P} \tag{1}$$

where $\mathbf{R}$ is the autocorrelation matrix of $\mathbf{x}'(n)$, $\mathbf{P}$ is the cross-correlation vector between $\mathbf{x}'(n)$ and $d(n)$. Due to the solution of inverse matrix, the computational burden and memory requirement of Eq. (1) challenge the controller for real-time implementation [22].

Consequently for real-time implementation, transfer functions $W(z)$ and $S(z)$, usually formed as FIR filters, are respectively expressed by coefficient vectors of impulse responses [22]:

$$\mathbf{W}(n) = [W_1(n), W_2(n), ..., W_L(n)]^T \tag{2a}$$

$$\mathbf{S}(n) = [S_1(n), S_2(n), ..., S_M(n)]^T \tag{2b}$$

where M and L are the length of $\mathbf{S}(n)$ and $\mathbf{W}(n)$, respectively. With Eq. (2), the transfer functions $W(z)$ and $S(z)$ become functions of time sequence n. Therefore the iterative LMS algorithm is utilized to update the coefficients of $\mathbf{W}(n)$ [23]

$$\mathbf{W}(n+1) = \mathbf{W}(n) + 2\mu e(n)\mathbf{x}'(n) \tag{3}$$

where μ is the step size, which characterizes the convergence speed of LMS [24]. The condition to guarantee the convergence of LMS algorithm is $0 < \mu < 1/\lambda_{\max}$, where $\lambda_{\max}$ is the maximum eigenvalue of $\mathbf{R}$ [25]. From Eq. (3), it is revealed that the coefficient vector at time $n+1$ is the summation of the coefficient vector at time n and a correction term, and the correction extent is decided by step size μ.

Yet, for step size there is a trade-off between the convergence speed of FxLMS algorithm and the stability of the control system [26]. Here stability refers to the ability of the controller to converge to the optimal solution or oscillate about it. Using large value of μ, the coefficient vector of FIR filter may suppress the vibration response effectively as soon as the controller is turned on, but it may diverge and then the spillover phenomenon occurs [27]. Although the stability can be guaranteed for small value of μ, the controller loses the capability to reduce the vibration response in a timely manner. Recently, the FxLMS algorithm with variable step sizes is utilized to balance the convergence speed and stability of control systems [28,29]. However, the computation burden of these methods is heavy [28,30,31], which may negatively influence the real-time performance of the control system due to lag effect. In order to achieve variable step size with the absence of computational challenges, the bang-bang control algorithm is introduced. Bang-bang controller can switch between two states and it is widely used for variable systems owning to simplicity and convenience [32–34]. In this work, the step size μ is adaptively tuned by bang-bang controller according to the feedback signal.

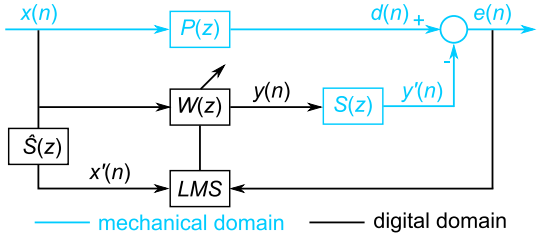

Fig. 1. Block diagram of classical FxLMS algorithm.

From Eq. (3), it is seen that apart from the step size μ of the filter $\mathbf{W}(n)$, both the estimated secondary path $\widehat{S}(z)$ and the reference signal $x(n)$ play important roles in the updates of the control vector. As described above, the dynamic characteristic of the vertical tail is time-varying, therefore the secondary path estimated offline is not applicable for real-time purpose [35]. Furthermore, the feedforward configuration to obtain reference signal is not available for aircrafts in flight. Consequently, the classical FxLMS algorithm cannot be used directly to alleviate the vibration of vertical tails. To overcome these challenges, the online identification of secondary path and the reconstruction of the reference signal are addressed in this paper as well.

This research is aimed to enhance the classical FxLMS algorithm to adaptively suppress the vibration of time-varying structures, and here the vertical tail of aircraft is investigated as a specific example. In the following section, multiple improvements on FxLMS algorithm, including online identification of secondary path, reconstruction of reference signal, and variable step size, are presented. Then numerical simulations are conducted to verify the feasibility and advantages of proposed enhancements. After that experimental investigations are used to further confirm its effectiveness. Finally, a summary is reported with conclusions.

2. Enhancements of classical FxLMS algorithm

In this section, the adaptive FxLMS algorithm is enhanced from the aspects of secondary path, reference signal, and step size μ for real-time vibration suppression of time-varying structures. In addition, the computational load and implementation considerations caused by these improvements are discussed.

2.1. Online identification of secondary path: simultaneous equation method

In recent years, numerous methods have been studied to identify the secondary path online. Most of them depend on the introduction of additional white noise [36–38]. Nevertheless, the mutual influences between the FxLMS controller and the modeling of secondary path always exist, which degrades the performance of both. Moreover, the vibration response caused by the injected noise cannot be suppressed by controllers since it is uncorrelated with the reference signal $x(n)$ [38,39]. To avoid such influences, the simultaneous equation method (SEM) that does not require injected noise is used here. In this method, another FIR filter $\mathbf{H}(n)$ of length Z is introduced to model the overall path $H(z)$ that is the superposition of primary path and secondary path. Jin et al. [22] have comprehensively studied this method, and the details are provided in Appendix for sake of being self-contained.

2.2. Reconstruction of reference signal

The ideal reference signal for FxLMS should be the unwanted vibration response $d(n)$ since the control signal needs to cancel it. However, $d(n)$ is not measurable in practice because it is superposed with the response of secondary path $y'(n)$. In the classical FxLMS, the upstream signal $x(n)$ is alternatively used to provide the information about the downstream $d(n)$, and that is why $x(n)$ is typically referred to as reference signal. Yet, feedforward configuration is not applicable for this research purpose. Therefore, the feedback structure shown in Fig. 2 serves for the reconstruction of the reference signal $d(n)$ based on feedback neutralization method [40].

The controlled residual vibration response is

$$e(n) = d(n) - y'(n) = d(n) - \mathbf{y}(n)\mathbf{S}(n) \tag{4a}$$

$$\mathbf{y}(n) = [\, y(n) \quad y(n-1) \quad \cdots \quad y(n-M+1) \,]^T \tag{4b}$$

In Eq. (4), the residual vibration response $e(n)$ and the output of controller $y(n)$ are measurable, and the secondary path has already been modeled online by SEM, so that the reference signal can be reconstructed as

$$\widehat{d}(n) = e(n) + \mathbf{y}(n)\widehat{\mathbf{S}}(n) \tag{5}$$

where $\widehat{d}(n)$ is the reconstructed reference signal.

2.3. Variable step size controlled by bang-bang algorithm

Bang-bang control is usually leveraged to change control systems from one state to the other. Here in order to balance the convergence speed and stability of the FxLMS system, bang-bang controller is integrated to adaptively switch the values of step size for $\mathbf{W}(n)$ based on feedback information. The implementation of bang-bang algorithm is straightforward: if the efficiency of controller cannot meet requirement of vibration suppression, the step size is switched to larger value to accelerate the convergence of control coefficients; otherwise the current coefficients are suitable, and consequently the smaller step size is adopted to maintain the stability of system by avoiding potential spillover phenomena. The criterion to evaluate the control performance is defined as

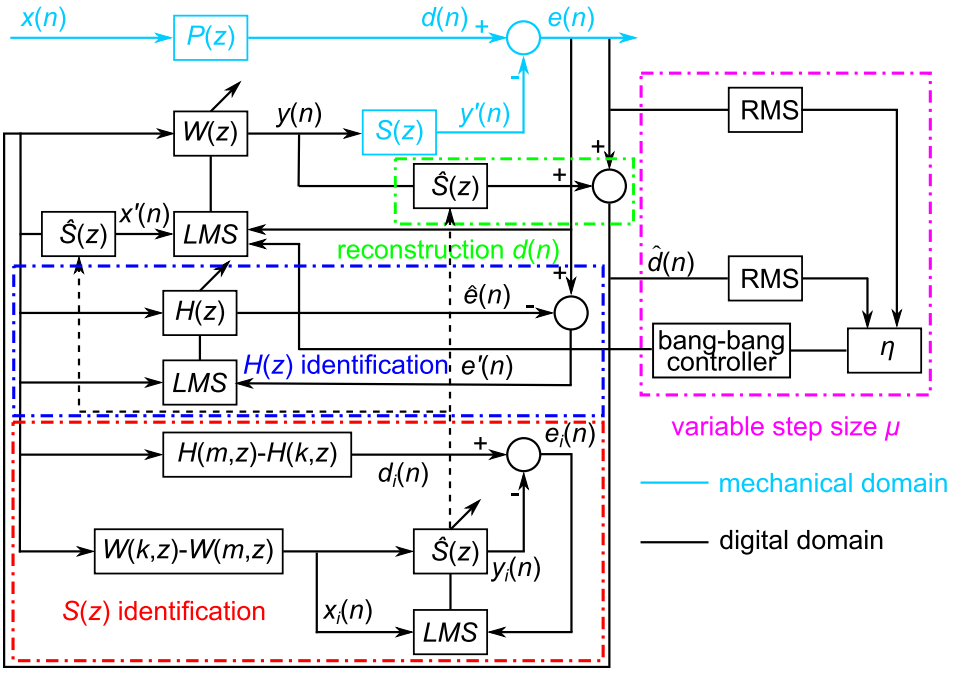

Fig. 2. Proposed FxLMS algorithm with online identification of secondary path, reconstruction of reference signal, and variable step size adjusted by bang-bang controller. The green box shows the reconstruction of reference signal, and the pink describes bang-bang controller. (For interpretation of the references to colour in this figure legend, the reader is referred to the web version of this article.)

$$\eta = \frac{e_{RMS}}{\widehat{d}_{RMS}} \tag{6}$$

where e_{RMS} and $\widehat{d}_{RMS}$ are the root-mean-squares (RMS) of the residual vibration response and reconstructed reference signal, respectively. The number of data points to compute RMS is N. The initial value of η is 1, which corresponds to the uncontrolled situation that $e(n)$ is $d(n)$.

According to the above discussion, the piecewise function of the step size μ for $\mathbf{W}(n)$ is defined as

$$\mu = \begin{cases} \mu_1 & \eta \leqslant \varphi \\ \mu_2 & \eta > \varphi \end{cases} \tag{7}$$

where μ_1 and μ_2 are constants ($\mu_1 < \mu_2$), and φ is the critical value of η ($\varphi < 1$). The step size μ_2 should satisfy $0 < \mu_2 < 1/\lambda_{\max}$ to guarantee the convergence of controller [25].

2.4. Operation procedures of proposed method

With all the enhancements described above, the overall operation procedures of the proposed method are summarized below

(1) At $n = 1$, the algorithm is initialized. The initial coefficients vectors of $\mathbf{H}(n)$ and $\mathbf{W}(n)$ are set to be $\mathbf{0}$ of corresponding lengths respectively, and that of $\widehat{\mathbf{S}}(n)$ is set to be $[a \quad 0 \quad \dots \quad 0]^T$ or $[0 \quad \dots \quad 0 \quad a]^T$ of corresponding lengths ($a \neq 0$).
(2) At time n, η (when $n \leqslant N$, $\eta = 1$) is obtained for the bang-bang controller, and the step size for $\mathbf{W}(n)$is adaptively adopted. Then $\mathbf{W}(n)$ and $\mathbf{H}(n)$ are updated respectively.
(3) The coefficients vector of $\widehat{\mathbf{S}}(n)$ is updated by SEM (see Appendix for details), and reference signal $\widehat{d}(n)$ is reconstructed.
(4) At time $n + 1$, repeat operations (2) and (3).

2.5. Computational load and implementation considerations

The computational load of control systems is important for performance assessment. Jin et al. [22] have reported the computational load of feed-forward FxLMS using SEM for online modeling of secondary path, in which the number of

multiplication/addition operations is $3Z + 3L + 3M$. For the proposed method shown in Fig. 2, the reconstruction of reference signal (i.e. Eq. (5)) adds M multiplication/addition operation. The bang-bang controller has $2N$ multiplication/addition operations, 3 division operation and 2 square root operation. Therefore, the computational load of bang-bang controller includes $3Z + 3L + 4M + 2N$ multiplication/addition operations, 3 division operation and 2 square root operation, which is increased compared with that in Ref. [22]. However, it is still far less than the computation limitation of CPU.

In terms of implementation considerations, the following factors are discussed here. Eq. (5) is derived on the hypothesis that $\widehat{\mathbf{S}}(n)$ is modeled ideally. However, estimation error always exists in the identified $\widehat{\mathbf{S}}(n)$, which is dependent on the assigned initial value. This may decrease the accuracy of reconstructed reference signal. Moreover, it is transferred to $\mathbf{H}(n)$ and further influences the modeling of $\widehat{\mathbf{S}}(n)$ in reverse way. As a consequence of iterations, the error may lead to divergence. Therefore, the initial vector of $\widehat{\mathbf{S}}(n)$ should be chosen appropriately to guarantee the convergence of FxLMS method. In fact, small a is less likely to cause divergence, while large a is favorable for control efficiency.

Another parameter N, the number of data points to compute e_{RMS} and $\widehat{d}_{RMS}$, also has great effects on the control efficiency and stability of controller. If N is too small, the update of η may fluctuate greatly which has negative influences on stability. On the other hand, if N is too large, η cannot reflect the real-time situation and the adaptation is harmed. Here N is decided by experiences.

In addition, the selection of critical value φ of bang-bang controller is influential. One limiting case is that when φ is smaller than the minimum η, the control system will diverge by keeping large step size. Therefore, the φ is set as 120% of the minimum value of η.

The initial wrong adaptations of $\widehat{\mathbf{S}}(n)$ and the reconstruction of reference signal have no effect on the online modeling of secondary path. The wrong adaptations of $\widehat{\mathbf{S}}(n)$ causes the wrong update of $\mathbf{W}(n)$, which results in the enlargement of $\mathbf{W}(n) - \mathbf{W}^*$ and further causes the magnification of $\Delta\mathbf{H}(n)$ and $\Delta\mathbf{W}(n)$ [22]. Then $\widehat{\mathbf{S}}(n)$ accelerates to the accurate value [22]. For the reconstruction of reference signal shown in Eqs. (4) and (5), the $\mathbf{y}(n)\widehat{\mathbf{S}}(n)$ and $\mathbf{y}(n)\mathbf{S}(n)$ are far less than residual vibration response $e(n)$ in the first few iterations. Therefore, Eqs. (4) and (5) can be simplified:

$$e(n) \approx d(n) \tag{8a}$$

$$\widehat{d}(n) \approx e(n) \tag{8b}$$

Substituting Eq. (8a) into (8b) and eliminating $e(n)$:

$$\widehat{d}(n) \approx d(n) \tag{9}$$

In addition to the above implementation considerations, there is an optimal tradeoff between robustness, performance and control saturation in the proposed method. The maximum variation range of secondary path is usually known in practice. Therefore, the designed controller should be stable for all secondary paths in this variation range firstly. Then, the control efficiency of controller should be improved as much as possible under the case of the actuator is not saturated.

3. Simulation studies

In order to verify the feasibility of the enhanced FxLMS controller described in Fig. 2, simulation studies are undertaken in MATLAB Simulink. The primary path $P(z)$ and secondary path $S(z)$ used here are identified from the experimental system shown in Fig. 8. Since the fundamental frequency of the vertical tail is 13.5 Hz, the sampling rate in Simulink is set as 1024 Hz that sufficiently satisfy Nyquist-Shannon theorem [41]. The identifications of primary path $P(z)$ and secondary path $S(z)$are implemented without additional weights. The input and output signals for modeling $P(z)$ are the excitation signal of the shaker and the root strain, respectively. In terms of $S(z)$, the input is changed to the driving signal sent to MFC actuators while the output is still the strain response. The measured signals are processed in MATLAB System Identification Toolbox to obtain the mathematic models of both paths [42].

3.1. Online identification of secondary path based on SEM

To confirm the advantages of SEM over noise-based methods for online identification of secondary path, FxLMS controllers with different identification methods are compared in Fig. 3. Here the control system is in feedforward configuration and the external disturbance, also the reference signal, is sinusoid of 13.5 Hz. The employed noise-based methods for comparison are respectively proposed by Eriksson, Bao, and Zhang since they are widely studied in literature [36–38]. The RMS of injected white noise is 10% of that of harmonic excitation. The primary and secondary path are both modeled with the FIR filter of length $M = 24$. The parameters used in all the methods are optimized by genetic algorithm. The sinusoidal responses

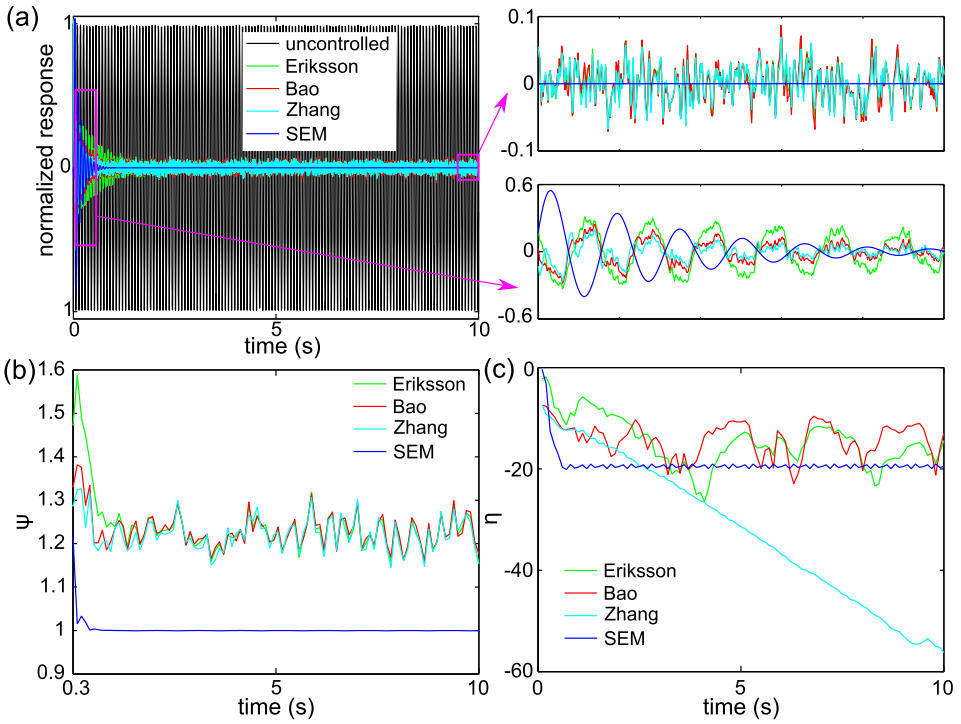

Fig. 3. Comparison of FxLMS controllers with different methods for online identification of secondary path. (a) Normalized peak values of sinusoidal response as the function of time. (b) Energy utilization ratio as the function of time. (c) Estimated error of secondary path as the function of time. The external disturbance is sinusoid of 13.5 Hz that is the natural frequency of first bending mode of the tail.

are plotted as the function of time in Fig. 3(a), and all the responses are normalized by the peak value of the uncontrolled response.

Considering Eriksson's method, the convergence speed of response is slower than that of other methods. The performance of FxLMS controller is improved by Bao and further improved by Zhang. However, the final residual responses in these methods are similar, around 0.07, which is caused by injected white noise. As a comparison, the response of SEM is suppressed by 100% within 1 s, and the controller performs stable to make the residual response close to 0. These comparisons reveal that SEM is more favorable to enhance the suppression performances of control systems.

In addition, the advantage of SEM is further confirmed by energy utilization ratio, which is presented as a function of time in Fig. 3(b). The energy utilization ratio describes the required energy for unit response suppression and its definition is

$$\psi = \frac{U}{\delta} \tag{10}$$

where U is the peak value of the controller output, and δ is the peak value reduction of sinusoid response.

In the first few steps, $\delta \approx 0$ since the response of open-loop and closed-loop is approximately equal, and then $U/\delta \to \infty$. Therefore, Fig. 3(b) only presents the energy utilization ratio ψ of controller between 0.3 s and 10 s. From Fig. 3(b), there exists significant fluctuations of ψ in Eriksson's method at 0.5 s. On the other hand, its maximum value is almost 60% of SEM, which indicates that it is not energy efficient. Although the energy efficiency is improved in both methods of Bao and Zhang at the beginning of simulation, the final energy utilization ratio ψ of injection white noise methods are also similar and the SEM method still has advantages over them.

The relative error η between the outputs of estimated and actual secondary paths is used here to evaluate the estimated error of secondary path in time domain, and its definition is:

$$\eta = 10\log_{10}\frac{\left|R_{\widehat{\mathbf{S}}} - R_{\mathbf{S}}\right|}{|R_{\mathbf{S}}|} \tag{11}$$

where $R_{\widehat{\mathbf{S}}}$ and $R_{\mathbf{S}}$ are the output of $\widehat{\mathbf{S}}(n)$ and $\mathbf{S}(n)$ respectively. The relative error is plotted in Fig. 3(c). It is observed that the relative error η of Eriksson's and Bao's method fluctuate greatly with time, which both indicate the secondary path is not identified well. The estimated performance of FxLMS controller is improved by Zhang, whose η can reach to -55 dB. For the SEM method, there is no fluctuation in the plotted time frame. Although the η of SEM is larger than that of Zhang's

method, it can meet the requirement of vibration control and its control performance has advantages over noised-based methods due to no injected white noise, which are reflected by minimizing residual response and energy utilization ratio.

3.2. Reconstruction of reference signal

The original and reconstructed reference signals in time domain are compared in Fig. 4, and all the signals are normalized by the maximum value of real reference signal. Since the first bending mode is specifically concerned here, the employed reference signal is white noise in the narrow band of [8 Hz, 16 Hz]. All the responses are normalized by the peak value of the real reference signal. From Fig. 4, it is observed that the reconstructed signal is in good agreement with the original, and the overall error is within 8.2%. Although the error is increased after 15 s, it still oscillates around zero and does not show diverging trend. From experiences it is found that the error of such extent is tolerable and the control system works well. This also confirms the efficacy of the secondary path in reverse way since the reconstruction depends on secondary path as shown in Eq. (5).

3.3. Parametric study for the update of $\mathbf{W}(n)$

Since the control performance is directly decided by $\mathbf{W}(n)$, its step size is adjusted by bang-bang controller. According to Eqs. (3) and (7), the update of coefficients vectors of $\mathbf{W}(n)$ depends on criterion value φ of bang-bang controller, step size μ of $\mathbf{W}(n)$, and length L of $\mathbf{W}(n)$. Therefore, the reduction ratio of response RMS of FxLMS controllers with different step size, length and φ is contrasted, shown in Fig. 5. The other parameters of controller are listed in Table 1. The disturbance is narrowband white noise excitation from 8 Hz to 16 Hz. The reduction ratio of response for divergent system is set as 0.

The fixed μ controller is used in Fig. 5(a), and the varied μ controlled by bang-bang controller is utilized in Fig. 5(b) and (c). From Fig. 5(a), it is seen that different lengths of $\mathbf{W}(n)$ have their own optimal step size, and the maximum reduction ratio is 44.1%. The relationship between optimal step size and optimal length can be approximated as a hyperbolic function as shown in Fig. 5(a). Moreover, the control system may be divergent if the large step size keeps for a long time, when the length is fixed. Considering the influence of criterion φ in Fig. 5(b) and (c), it is found that an appropriate φ can improve the

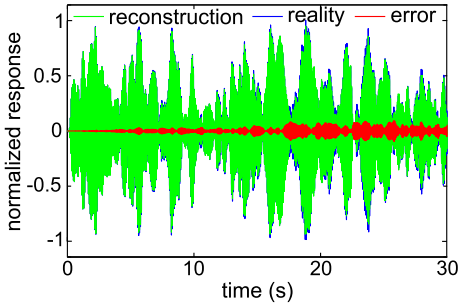

Fig. 4. Original reference signal $d(n)$, reconstructed reference signal $\widehat{d}(n)$, and the reconstruction error $\widehat{d}(n) - d(n)$ in time domain. All the signals are normalized by the maximum value. The excitation signal is narrowband white noise from 8 Hz to 16 Hz which covers the first bending mode of the vertical tail.

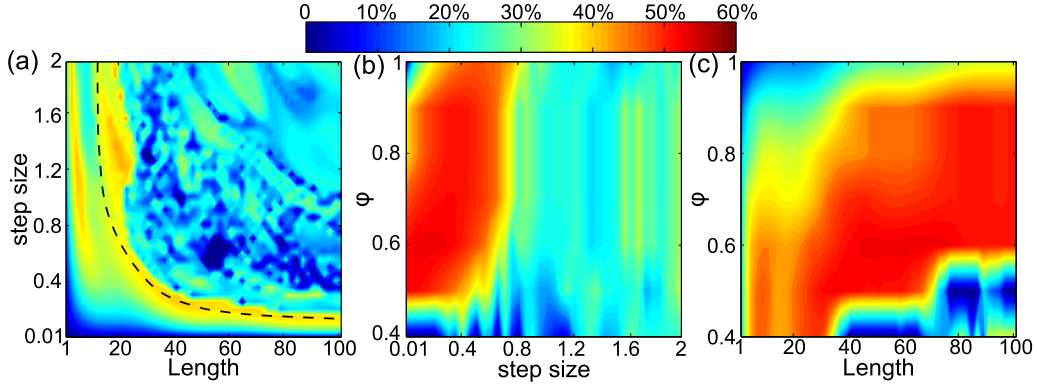

Fig. 5. Reduction ratio of response RMS of FxLMS controllers with different step size, length and the criterion φ for control efficiency. (a) Relationship between step size and length. (b) Relationship between step size and φ. (c) Relationship between length and φ. The excitation signal is narrowband white noise excitation from 8 Hz to 16 Hz. The fixed μ controller is used in (a), and the bang-bang controller is utilized in (b) and (c).

Table 1
Parameters of FIR filter using LMS algorithm.

Filter length			Step size			Initial value of filter weights		
$\mathbf{W}(n)$	$\mathbf{H}(n)$	$\mathbf{S}(n)$	$\mathbf{W}(n)$	$\mathbf{H}(n)$	$\mathbf{S}(n)$	$\mathbf{W}(n)$	$\mathbf{H}(n)$	$\mathbf{S}(n)$
50	42	36	0.1\1.6	0.02	0.2	**0**	**0**	[0, 0,. . .,0.1]

performance of controller. As φ is around 0.6, the reduction ratio of response reaches maximum. When the bang-bang controller is implemented, the maximum reduction ratio of controller is improved from 44.1% to 53.8%, which indicates the necessity of bang-bang control on FxLMS method.

3.4. Variable step size adjusted by bang-bang algorithm

The online identification and reconstruction of reference signal have been investigated above, but the efficiency of the collaboration of FxLMS and bang-bang has not been explored yet. In Fig. 6, the FxLMS controller with fixed step size is contrasted with that whose step size is adjusted by bang-bang algorithm, and all the responses are normalized by the peak value of the uncontrolled response. Fig. 6(a) and (c) present the output of FxLMS controller, and Fig. 6(b) and (d) demonstrate the corresponding vibration alleviation results. The external disturbance is sinusoid of 13.5 Hz that is the natural frequency of the first-order mode of the vertical tail. The secondary path is the discrete transfer function of the vertical tail model. The parameters of this proposed algorithm are defined as: $N = 1000$, and $\varphi = 0.6$ in the simulation, and the other parameters are shown in Table 1.

For the FxLMS controller with fixed step size in Fig. 6(a), it is observed that the output of fixed μ controller is close to zero at the beginning, which indicates that it converges slowly. For the bang-bang controller, the output reaches to 0.63 at 1.5 s, while as the direct contrast the corresponding value of fixed μ is only 0.025 at the same time. After that the controller output of $\mathbf{W}(n)$ with fixed μ gradually increases and it accelerates to the optimum value. As a result, the response suppression is enhanced as shown in Fig. 6(b). But for the collaboration of FxLMS and bang-bang, the system switches to smaller μ to guarantee the stability of the system when the vibration is controlled by 73%. Consequently, the output of bang-bang controller is gradually decreased to the optimum objective to maintain the high level of suppression performance. The final control efficiency and output of collaborative system are almost the same as those of controller with fixed μ. Moreover, the phase difference θ between the response of identified secondary path and that of real secondary path is also similar, about 14.6°. This simulation study demonstrates that the system whose step size is adjusted by bang-bang algorithm can respond much more

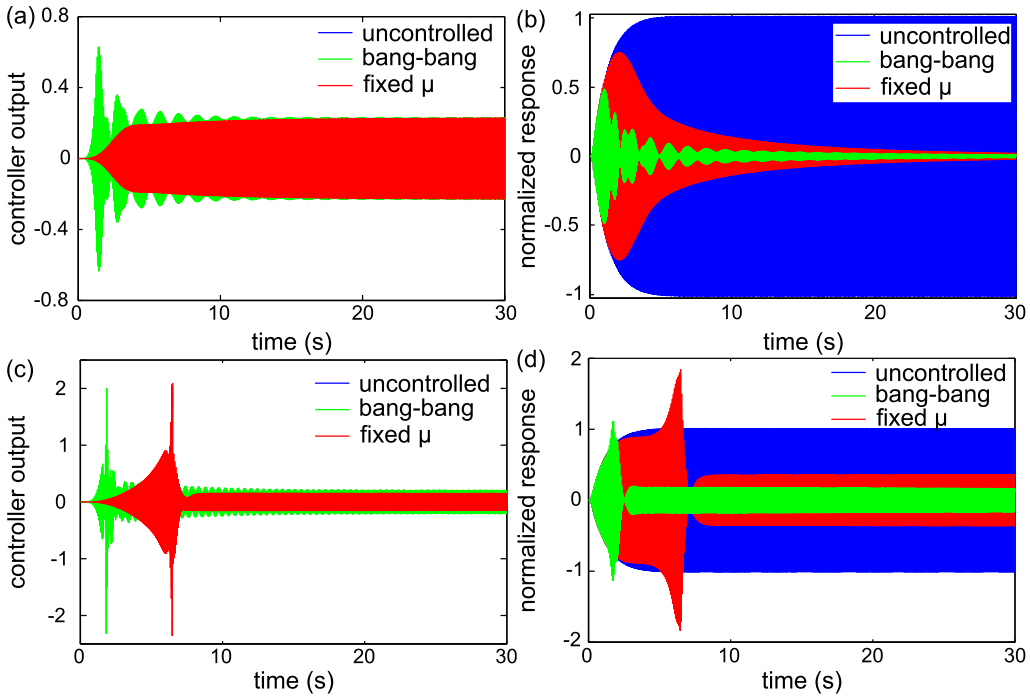

Fig. 6. Performance of the FxLMS controller under sinusoid excitation of 13.5 Hz. (a) Output of FxLMS controller. (b) Vibration suppression performance of FxLMS controller. (c) Output of FxLMS controller under the phase shift. (d) Vibration suppression performance of FxLMS controller under the phase shift.

quickly than fixed step size at the beginning. In addition, once the vibration is suppressed to a satisfying extent, the step size of the system is decreased to maintain the stability of the control system while the suppression performance is not degraded.

The FxLMS method can converge due to the robustness of the method itself, if the phase estimation error is less than 90° [43]. In order to verify the influence of the phase difference θ on the performance of controller, an all-pass filters is utilized in the simulation to increase the phase difference θ to close to 90°, as shown in Fig. 6(c) and (d). It can be seen that the control system is still stable even if the phase difference θ is close to 90°. Similar to the results of Fig. 6(a) and (b), the convergence speed of the bang-bang controller has advantage over that of fixed μ controller. Moreover, the spillover of response and the residual vibration response are also decreased 39.6% and 46.1% respectively.

3.5. Sudden change of secondary path

In order to further demonstrate the robustness of the proposed method, the simulation that the secondary path is changed suddenly is implemented, shown in Fig. 7. The external force in this section is narrowband white noise excitation from 8 Hz to 16 Hz. At 40 s, the additional weight is added on the tip of the vertical tail to shift the natural frequencies of the structure, shown in Fig. 8. The original model is named as model A and the one with additional weight is named as model B. The parameters of controller are listed in Table 2. From Fig. 7(a), it can be seen that after the coefficients of bang-bang controller are convergent, the reduction ratio of response RMS of model A is 51.6% between 20 s and 40 s, and the response RMS of model B is decreased by 48.4% between 60 s and 80 s. Yet, these of fixed μ controller are 30.8% and 37.4% respectively. Moreover, the output of bang-bang controller is also larger than that of fixed μ controller in Fig. 7(b). After the coefficients of bang-bang controller are convergent, the energy utilization ratio ψ for model A and model B is 0.258 and 0.271 respectively. Therefore, the sudden change of secondary path has little effect on the efficiency of the proposed controller.

From Fig. 7(c), it is observed that the frequency characteristic of identified secondary path using bang-bang controller is more suitable to that of actual secondary path, compared with fixed μ. For model A, the error of response RMS of identified secondary path related to the response RMS of real secondary path is 34.5%, and that for model B is 33.2%. The peak error of amplitude-frequency characteristic for model A and model B is 2.71 dB and 2.85 dB respectively. Although the response error of identified secondary path using feedback SEM method is larger than that using feed-forward SEM method, the phase difference θ under the sinusoidal excitation from 8 Hz to 16 Hz is less than 90°, shown in Fig. 7(d), which guarantees the stability of FxLMS system [43].

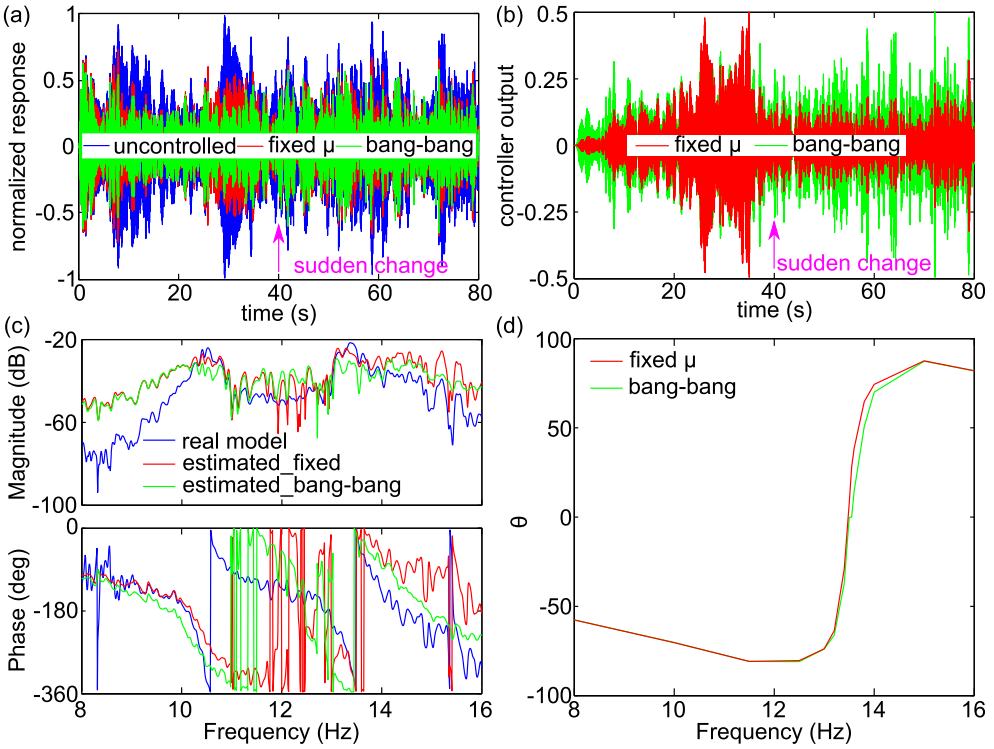

Fig. 7. Performance of the proposed controller under the sudden change of secondary path during adaptation process. (a) Vibration suppression performance. (b) Controller output. (c) Bode diagram of transfer function of secondary path. The frequency band of narrowband white noise excitation is from 8 Hz to 16 Hz. (d) Phase different θ under the sinusoidal excitation with different frequency for model A.

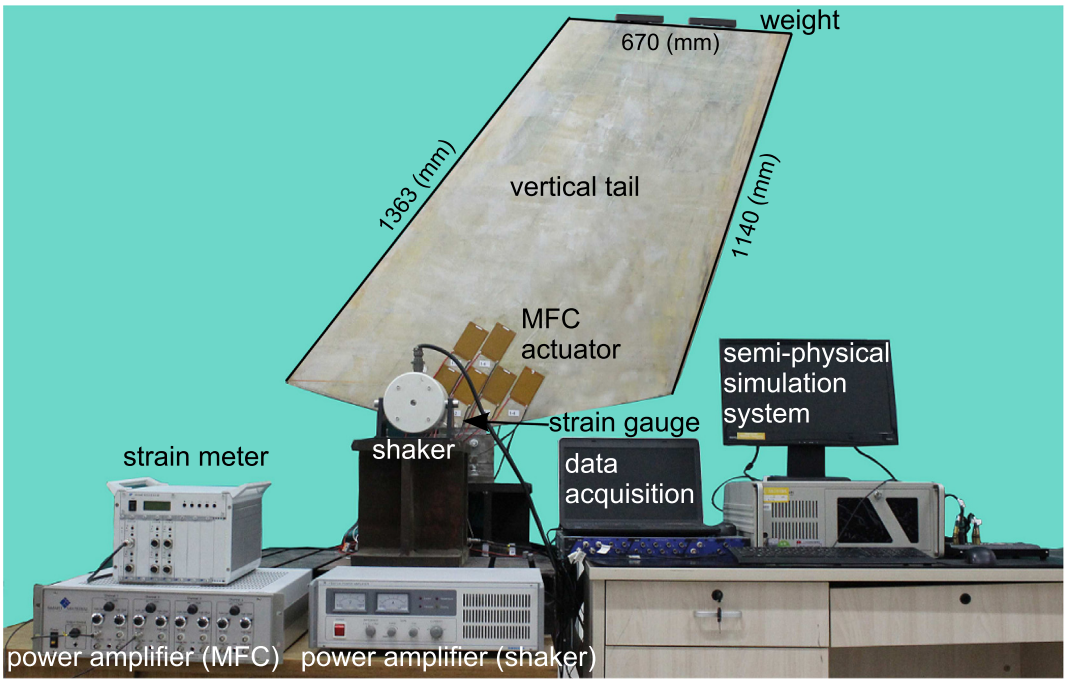

Fig. 8. Overview of experimental setup of adaptive buffeting suppression system using MFC actuators.

Table 2
Parameters of FIR filter for sudden change of secondary path.

Filter length			Step size			Initial value of filter weights		
$\mathbf{W}(n)$	$\mathbf{H}(n)$	$\mathbf{S}(n)$	$\mathbf{W}(n)$	$\mathbf{H}(n)$	$\mathbf{S}(n)$	$\mathbf{W}(n)$	$\mathbf{H}(n)$	$\mathbf{S}(n)$
50	42	36	0.17\1.17	0.45	0.88	**0**	**0**	[0, 0,. . .,0.1]

4. Experimental investigations

In this section, a series of vibration control experiments are conducted to validate the feasibility of the proposed algorithm described in Fig. 2. The parameters of proposed algorithm are defined as: $\mu_1 = 0.1$, $\mu_2 = 1.6$, and $\varphi = 0.6$. The sampling point N of the RMS solving modules is set as 3000, in order to reduce the influence of noise. As it is expected to control the first-order bending mode of the vertical tail, a discrete band-pass filter from 5 Hz to 20 Hz is used prior to the input of controller to eliminate noise.

4.1. Experimental setup and system identification

The adaptive system to suppress the vibration of the vertical tail is presented in Fig. 8. This system is in single-input-single-output configuration aiming for the first mode of the vertical tail since its threats are the most severe [44]. The external excitation signal from the real-time semi-physical simulation system (Quarc, Quanser) is applied to the vertical tail via the power amplifier (YE5872A, Sinocera) and the shaker (JZK-10, Sinocera). The strain at the tail root is selected as the feedback signal and it is measured by the dynamic strain meter (DH3840, Donghua). Then the strain is sent to the digital controller in the semi-physical system. The generated control signal is amplified by the high voltage amplifier (HVA 1500/50-4, Smart Material Corp.) to actuate the Macro Fiber Composites (MFC, M8557-P1, Smart Material Corp) for vibration suppression. There are two reasons to choose MFC as the actuator: one is that its electromechanical coefficient is high for actuation, the other is that its flexibility enables it to conform to the curved surface of the tail [45,46]. Although there are multiple MFC patches, they are connected in parallel which only requires single input. All the data are acquired by the Vibrunner (m + p international) and the acquisition rate is 1024 Hz. The additional weights (steel) on the tip of the vertical tail are used to shift the fundamental frequency from 13.5 Hz to 10.5 Hz to realize varying structures.

4.2. Comparison of FxLMS controllers with variable and fixed step size

The FxLMS controller whose step size is adjusted by bang-bang algorithm is contrasted to the FxLMS with fixed step size to validate the effectiveness of variable step size using the original vertical tail, shown in Fig. 9. Similar to the external excitation in Section 3, the frequency of sinusoid excitation is 13.5 Hz and the frequency band of noise excitation is from 8 Hz to 16 Hz. Considering Fig. 9(a), it is seen that the response of the proposed algorithm is decreased by 88.7% within 4 s and decreased by 92.0% within 10 s. As a direct contrast, the case of fixed step size is only decreased by 32.4% and 79.3%, respectively. This distinction in control performance demonstrates that the proposed method is able to reduce the vibration response more promptly than the FxLMS with fixed step size, whose reason is that the controller coefficients of the proposed FxLMS can reach to optimum objective faster. From Fig. 9(b), it is seen that the random response is suppressed effectively by both fixed and variable step size FxLMS controllers. However, if the fixed size step μ is replaced by variable step size, the reduction of PSD peak reaches to 13.11 dB and the reduction rate of response RMS reaches to 53.3%, while those of the FxLMS with fix step size are 5.25 dB and 30.3% respectively. Results indicate that the performance of FxLMS controller is improved by variable step size, especially in the resonance frequency band.

4.3. Comparison of FxLMS controllers with online and offline identified secondary path

The proposed FxLMS controller is contrasted to the feedback FxLMS with offline identified secondary path to validate the efficiency of the online identification of secondary path for time-varying vertical tail in Fig. 10. The variations of the vertical tail are owing to the additional weights that shift the natural frequencies, as shown in Fig. 8. In this experiment, the frequency of sinusoid excitation is the natural frequency of the structural first-order mode, i.e. 13.5 Hz in Fig. 10(a) and 10.5 Hz in Fig. 10(b) respectively; the frequency band of white noise excitation in Fig. 10(c) and (d) is from 8 Hz to 16 Hz. From Fig. 10(a) and (c), it is seen that for the vertical tail without additional weights, the vibration response is suppressed effectively by both offline and online identification FxLMS controllers. The peak values of the sinusoid response are decreased by 92.7% and 92.0% within 10 s, the peak values of the PSD are decreased by 14.26 dB and 13.13 dB, and the RMS value of random response are decreased by 61.3% and 53.3%, respectively. However, when the system characteristics is changed by the additional weights in Fig. 10(b) and (d), the performance of the offline identification FxLMS controller is degraded significantly. The peak value of the sinusoid response is increased by 99.3% within 10 s and the peak value of the PSD is also increased by 0.26 dB, which indicates that the system is divergent. Nevertheless, the performance of the proposed FxLMS for the vertical tail with additional weights is similar to that for the original vertical tail. Therefore, the proposed FxLMS is enabled to adapt to the change of system characteristics by the online identification of secondary path. Results indicate that the proposed algorithm has an advantage over offline identification FxLMS to control the vibration response of time-varying structure.

4.4. Robustness of enhanced FxLMS controller under impulsive disturbance and time-varying system

Robustness is an important criterion to evaluate control system. Robustness refers to that the control system can maintain certain performance under disturbances, which is used to characterize the stability of control system to the uncertainties [47]. For vibration control considered here, the terminology refers to the capability of the system to maintain the effectiveness of vibration suppression.

Among various disturbances, the impulsive excitation threats the stability of the control system most severely [48]. Consequently in order to examine the robustness of proposed algorithm, the addition weights are suddenly attached to the vertical tail by magnetic force, which is considered as impulsive excitation. After that the additional weights serve to shift the natural frequency of the vertical tail. As shown in Fig. 11, the vibration response of the vertical tails has been

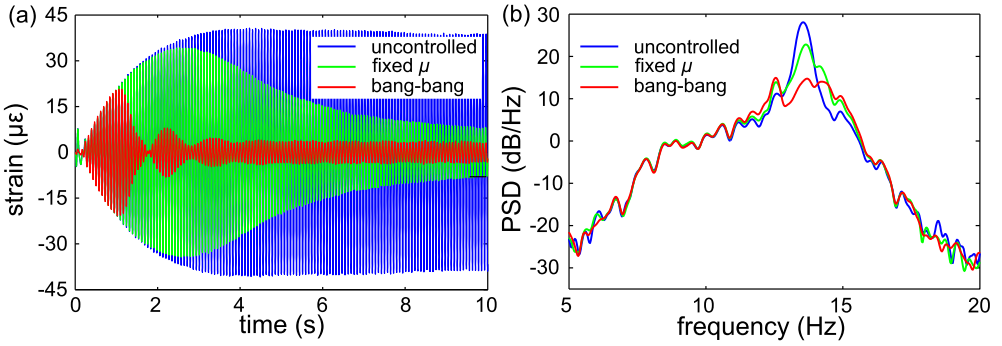

Fig. 9. Vibration suppression performance of the proposed FxLMS controllers. (a) Under sinusoid excitation of 13.5 Hz (b) under narrowband white noise excitation from 8 Hz to 16 Hz.

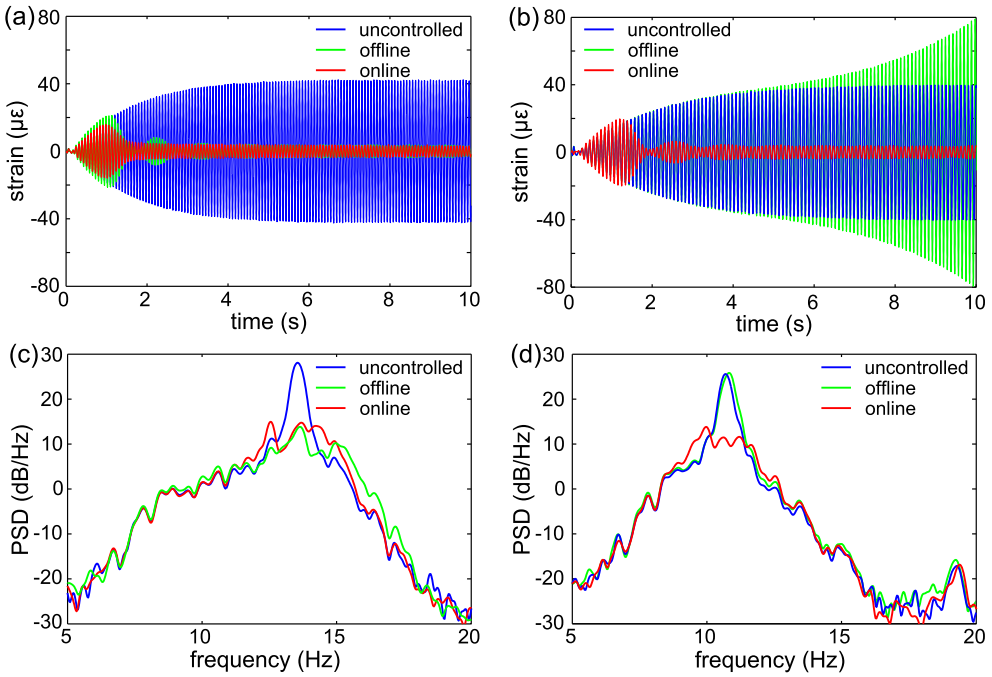

Fig. 10. Vibration suppression performance of FxLMS controllers under sinusoid excitation. (a) Vertical tail without additional weights, sinusoid excitation of 13.5 Hz (b) Vertical tail with additional weights, sinusoid excitation of 10.5 Hz. Vibration suppression performance of FxLMS controllers under narrowband white noise excitation from 8 Hz to 16 Hz. (c) Vertical tail without additional weights (d) Vertical tail with additional weights.

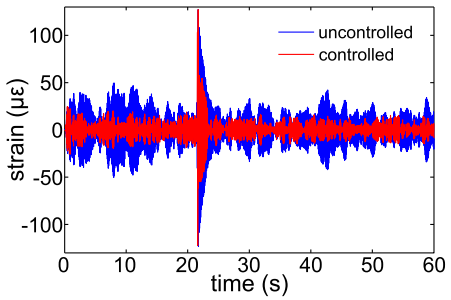

Fig. 11. Vibration suppression performance of the proposed FxLMS controller under narrowband white noise excitation from 8 Hz to 16 Hz. The strain response is jump when the additional weights are applied.

alleviated to satisfying extent and then a sharp increase of response appears due to the sudden attachment of weights. It is observed that the response peak of the closed-loop system is the same as that of the open-loop system, which means that the proposed method is not disturbed to divergence by the impulsive excitation. Furthermore, the strain is decreased greatly by the control system immediately after the magnetic impulse, and this validates the robustness of proposed method. For the time series in Fig. 11, the RMS of the response is decreased by 56.37% within 20 s, and it is decreased by 52.66% between 40 s and 60 s. This comparison demonstrates the efficiency of the proposed method remains on the same level although the natural frequency of the first-order mode is decreased by 22%. The above results indicate that the enhanced FxLMS controller is robust to the impulsive disturbance and time-varying system.

5. Conclusions

An enhanced FxLMS controller with online modeling of secondary path and adaptively adjusted step size is developed in this work. The online identification of secondary path based on SEM is implemented to capture the change of the dynamic characteristics of structure in real-time. And the adaptation of step size by bang-bang algorithm is used to balance the efficiency and stability of FxLMS algorithm. The feasibility of this method is validated by numerical simulation as well as

experiment. Here the vertical tail under buffeting loading is studied as the representative of time-varying structure. The results demonstrate that the proposed method is able to reduce the vibration response more effectively than FxLMS with fixed step size, and it is adaptive to the varying characteristics of vibrating structure. The enhanced FxLMS controller is confirmed as an effective method to suppress the vibration of time-varying system due to the evident improvements on control efficient and system stability numerically and experimentally.

Acknowledgement

The authors would like to acknowledge the financial support by the National Natural Science Foundation of China (No. 11872312 and No. 11502208) and Natural Science Basic Research Plan in Shaanxi Province of China (No. 2018JM5179).

Appendix

The simultaneous equation method (SEM) has been studied by Jin et al. in Ref. [22], and its detailed theory is covered here for the convenience of readers.

The block diagram of SEM is illustrated in Fig. A.1 [22]. The reference signal is used as the input of identification system to simplify the active control system, since the system identification is separated from the control system. In this method, the overall path from the reference signal to the residual response is defined as $H(z)$, which is the superposition result of primary path and secondary path. For any case, ideally the overall path can be modeled accurately by

$$H(z) = P(z) - W(z)S(z) \tag{A.1}$$

During the iteration process of the filters $W(z)$ and $H(z)$, the coefficients are uncorrelated at different iterating steps. $W(n-m,\ z)$ and $W(n-k,\ z)$ are selected at different time steps $n-m$ and $n-k$, respectively (where $m = 0, 1, 2...;\ k = 0, 1, 2...;\ m \neq k$). As a result, two independent equations are obtained as

$$H(n-m,\ z) = P(z) - W(n-m,\ z)S(z) \tag{A.2a}$$

$$H(n-k,\ z) = P(z) - W(n-k,\ z)S(z) \tag{A.2b}$$

It is assumed that $k < m$ and the dynamic characteristics of the secondary and primary path are not change between the time m and k. Combing Eq. (A.2) and eliminating $P(z)$ yields

$$S(z) = \frac{H(n-m,\ z) - H(n-k,\ z)}{W(n-k,\ z) - W(n-m,\ z)} \tag{A.3}$$

if $W(n-k,\ z) \neq W(n-m,\ z)$. And the filter $H(z)$ is also formed as FIR filter, whose coefficients is

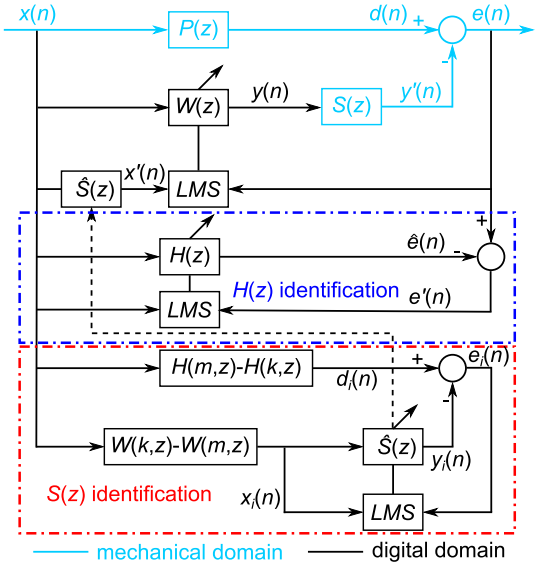

Fig. A.1. Feedforward FxLMS algorithm with online identification of secondary path based on SEM. The blue rectangle denotes the identification of the overall path $H(z)$, and the red is used to identify the secondary path $S(z)$. (For interpretation of the references to colour in this figure legend, the reader is referred to the web version of this article.)

$$\mathbf{H}(n) = [H_1(n), H_2(n), ..., H_Z(n)] \tag{A.4}$$

where Z is the filter length.

From Eq. (A.3), it is shown that $H(n-m,\ z) - H(n-k,\ z)$ is the product of $S(z)$ and $W(n-k,\ z) - W(n-m,\ z)$. In Fig. A.1, an adaptive filter $\widehat{S}\ (z)$ is introduced and its coefficients are updated by LMS algorithm to make $H(n-m,\ z) - H(n-k,\ z)$ equal to the product of $W(n-k,\ z) - W(n-m,\ z)$ and $\widehat{S}\ (z)$. The estimated $\widehat{S}\ (z)$ is expected to converge to $S(z)$ with some error. Since all adaptive filter coefficients are simultaneously undated, the estimation error from $H(n-m,\ z) - H(n-k,\ z)$ is widely and uniformly distributed over the coefficients, and so the errors is not divergent. In fact, $\widehat{S}\ (z)$ converges on:

$$\widehat{S}\ (z) = S(z) + S'(n,z) + R(n,z) \tag{A.5}$$

where $S'(n,z)$ is the identification error of $\widehat{S}\ (z)$, and $R(n,z)$is the estimation error of $H(n-m,\ z) - H(n-k,\ z)$. The estimation precision of $S(z)$ is limited to an extent due to the inherent estimation error $R(n,z)$. As a matter of fact, only the secondary path model in the frequency band of reference signal can be obtained.

In Fig. A.1, it is observed that there are three FIR filters: $\mathbf{W}(n)$ for the update of coefficients of controller, $\mathbf{H}(n)$ for the online modelling of overall path, and $\widehat{\mathbf{S}}\ (n)$ for the online identification of secondary path. The updating equation of $\mathbf{H}(n)$ is shown as:

$$\mathbf{H}(n+1) = \mathbf{H}(n) + \mu_H \mathbf{x}(n) e'(n) \tag{A.6}$$

where μ_H is the step size of filter $\mathbf{H}(n)$,

$$e'(n) = e(n) - \widehat{e}\ (n) = d(n) - y'(n) - \mathbf{x}^T(n)\mathbf{H}(n) \tag{A.7}$$

The updating equation of $\widehat{\mathbf{S}}\ (n)$ is:

$$\widehat{\mathbf{S}}\ (n+1) = \widehat{\mathbf{S}}\ (n) + \mu_S \mathbf{x}_i(n) e_i(n) \tag{A.8}$$

where μ_S is the step size of filter $\widehat{\mathbf{S}}\ (n)$,

$$\mathbf{x}_i(n) = [\, x_i(n) \quad x_i(n-1) \quad \cdots \quad x_i(n-M+1)\,]^T \tag{A.9}$$

$$e_i(n) = d_i(n) - y_i(n) = d_i(n) - \mathbf{x}_i^T(n)\ \widehat{\mathbf{S}}\ (n) \tag{A.10}$$

$$d_i(n) = \mathbf{x}^T(n)\Delta\mathbf{H}(n) \tag{A.11}$$

$$x_i(n) = \mathbf{x}^T(n)\Delta\mathbf{W}(n) \tag{A.12}$$

where $\Delta\mathbf{H}(n) = \mathbf{H}(n-m) - \mathbf{H}(n-k)$, $\Delta\mathbf{W}(n) = \mathbf{W}(n-k) - \mathbf{W}(n-m)$.

References

[1] S. Rao, Mechanical Vibrations, fourth ed., Pearson Prentice Hall, Upper Saddle River, New Jersey, 2004.
[2] C. Hansen, S. Snyder, X. Qiu, L. Brooks, D. Moreau, Active Control of Noise and Vibration, CRC Press, Boca Raton, 2012.
[3] D.A. Bies, C.H. Hansen, C.Q. Howard, Engineering Noise Control, fifth ed., CRC Press, Boca Raton, 2017.
[4] D.X. Phu, T.D. Huy, V. Mien, S.B. Choi, A new composite adaptive controller featuring the neural network and prescribed sliding surface with application to vibration control, Mech. Systems Signal Process. 107 (2018) 409–428.
[5] J. Lu, P. Wang, Z. Zhan, Active vibration control of thin-plate structures with partial SCLD treatment, Mech. Syst. Signal Process. 84 (2017) 531–550.
[6] A.R. Tavakolpour-Saleh, M.A. Haddad, A fuzzy robust control scheme for vibration suppression of a nonlinear electromagnetic-actuated flexible system, Mech. Syst. Signal Process. 86 (2017) 86–107.
[7] B.H. Beam, A.E. Lopez, V.D. Reed, Wind-tunnel Measurements at Subsonic Speeds of the Static and Dynamic-rotary Stability Derivatives of a Triangular-wing Airplane Model Having a Triangular Vertical Tail, National Advisory Committee for Aeronautics, Washington, 1955.
[8] I. Gursul, Unsteady flow phenomena over delta wings at high angle of attack, AIAA J. 32 (1994) 225–231.
[9] B.H. Lee, Vertical tail buffeting of fighter aircraft, Prog. Aerospace Sci. 36 (2000) 193–279.
[10] R. Moses, Vertical tail buffeting alleviation using piezoelectric actuators – some results of the actively controlled response of buffet-affected tails (ACROBAT) program, in: Proc. of SPIE, Vol. 3044, San Diego, 1997.
[11] B. Chomette, D. Remond, S. Chesne, L. Gaudiller, Semi-adaptive modal control of on-board electronic boards using an identification method, Smart Mater. Struct. 17 (2008) 065019.
[12] P. Ambrosio, G. Cazzulani, F. Resta, F. Ripamonti, An optimal vibration control logic for minimising fatigue damage in flexible structures, J. Sound Vibr. 333 (2014) 1269–1280.
[13] F. Ripamonti, G. Cazzulani, S. Cinquemani, F. Resta, A. Torti, Adaptive active vibration control to improve the fatigue life of a carbon-epoxy smart structure, in: Active and Passive Smart Structures and Integrated Systems, San Diego, 2015.
[14] H.F. Genari, N. Mechbal, G. Coffignal, E.G. Nóbrega, A reconfigurable damage-tolerant controller based on a modal double-loop framework, Mech. Syst. Signal Process. 88 (2017) 334–353.
[15] H.F. Genari, N. Mechbal, G. Coffignal, E.G. Nóbrega, Damage-tolerant active control using a modal H∞-norm-based methodology, Control Eng. Practice 60 (2017) 76–86.

[16] C. Zou, B. Li, L. Liang, W. Wang, Active vertical tail buffeting suppression based on macro fiber composites, in: Proc. of SPIE, Vol. 9803, Las Vegas, 2016.
[17] G. Jin, X. Liu, Z. Liu, T. Yang, Active control of structurally radiated sound from an elastic cylindrical shell, J. Mar. Sci. Appl. 10 (2011) 88–97.
[18] Z. Gao, X. Zhu, Y. Fang, H. Zhang, Active monitoring and vibration control of smart structure aircraft based on FBG sensors and PZT actuators, Aerospace Sci. Technol. 63 (2017) 101–109.
[19] Z. Gan, A. Hillis, J. Darling, Adaptive control of an active seat for occupant vibration reduction, J. Sound Vibr. 349 (2015) 39–55.
[20] S. Prakash, T.R. Kumar, S. Raja, D. Dwarakanathan, H. Subramani, C. Karthikeyan, Active vibration control of a full scale aircraft wing using a reconfigurable controller, J. Sound Vibr. 361 (2016) 32–49.
[21] B. Widrow, J. Glover, J. McCool, J. Kaunitz, C. Williams, R. Hearn, J. Zeidler, J. Dong, R. Goodlin, Adaptive noise cancelling: principles and applications, in: Proceedings of the IEEE, vol. 63, pp. 1692–1716, 1975.
[22] G. Jin, T. Yang, Y. Xiao, Z. Liu, A simultaneous equation method-based online secondary path modeling algorithm for active noise control, J. Sound Vibr. 303 (2007) 455–474.
[23] R. Martinek, R. Kahankova, H. Nazeran, J. Konecny, J. Jezewski, Non-invasive fetal monitoring: a maternal surface ECG electrode placement-based novel approach for optimization of adaptive filter control parameters using the LMS and RLS algorithms, Sensors 17 (2017) 1154.
[24] V.E. DeBrunner, D. Zhou, Hybrid filtered error LMS algorithm: another alternative to filtered-x LMS, IEEE Trans. Circuits Systems I: Regular Papers 53 (2006) 653–661.
[25] B. Krstajic, Z. Zecevic, Z. Uskokovic, Increasing convergence speed of FxLMS algorithm in white noise environment, AEU-Int. J. Electron. Commun. 67 (2013) 848–853.
[26] Z. Qiu, C.M. Lee, Z.H. Xu, L.N. Sui, A multi-resolution filtered-x LMS algorithm based on discrete wavelet transform for active noise control, Mech. Syst. Signal Process. 66 (2016) 458–469.
[27] L. Vicente, Novel FxLMS convergence condition with deterministic reference, IEEE Trans. Signal Process. 54 (2006) 3768–3774.
[28] B. Huang, Y. Xiao, J. Sun, G. Wei, A variable step-size FXLMS algorithm for narrowband active noise control, IEEE Trans. Audio Speech Language Process. 21 (2013) 301–312.
[29] D. Chang, F. Chu, A new variable tap-length and step-size FxLMS algorithm, IEEE Signal Process. Lett. 20 (2013) 1122–1125.
[30] M.T. Akhtar, M. Abe, M. Kawamata, A new variable step size LMS algorithm-based method for improved online secondary path modeling in active noise control systems, IEEE Trans. Audio Speech Language Process. 14 (2006) 720–726.
[31] A. Zeb, A. Mirza, Q.U. Khan, S.A. Sheikh, Improving performance of FxRLS algorithm for active noise control of impulsive noise, Appl. Acoustics 116 (2017) 364–374.
[32] H. Yan, Y. Zhu, Bang–bang control model for uncertain switched systems, Appl. Math. Model. 39 (2015) 2994–3002.
[33] H. Yan, Y. Zhu, Bang–bang control model with optimistic value criterion for uncertain switched systems, J. Intelligent Manuf. 28 (2017) 527–534.
[34] Y. Wang, D.J. Inman, Comparison of control laws for vibration suppression based on energy consumption, J. Intell. Mater. Syst. Struct. 22 (2011) 795–809.
[35] S.M. Kuo, D. Vijayan, A secondary path modeling technique for active noise control systems, IEEE Trans. Speech Audio Process. 5 (1997) 374–377.
[36] L.J. Eriksson, M.C. Allie, Use of random noise for on-line transducer modeling in an adaptive active attenuation system, J. Acoustical Soc. Am. 85 (1989) 797–802.
[37] C. Bao, P. Sas, H. Van Brussel, Adaptive active control of noise in 3-D reverberant enclosures, J. Sound Vibr. 161 (1993) 501–514.
[38] M. Zhang, H. Lan, W. Ser, A robust online secondary path modeling method with auxiliary noise power scheduling strategy and norm constraint manipulation, IEEE Trans. Speech Audio Process. 11 (2003) 45–53.
[39] H. Lan, M. Zhang, W. Ser, An active noise control system using online secondary path modeling with reduced auxiliary noise, IEEE Signal Process. Lett. 9 (2002) 16–18.
[40] K. Chen, Active Noise Control, second ed., National Defense Industry Press, Beijing, 2014.
[41] C.L. Farrow, M. Shaw, H. Kim, P. Juhas, S.J.L. Billinge, The Nyquist-Shannon sampling theorem and the atomic pair distribution function, Phys. Rev. B 84 (2011) 4578–4586.
[42] L. Ljung, R. Singh, Version 8 of the MATLAB system identification toolbox, IFAC Proc. Vol. 45 (2012) 1826–1831.
[43] X. Sun, D. Chen, Convergence analysis of filtered-X LMS algorithm with secondary path modeling error, Acta Acustica 27 (2002) 97–101.
[44] A. Preumont, Vibration Control of Active Structures: An Introduction, Springer Science & Business Media, London, 2002.
[45] A. Kovalovs, Application of macro-fiber composite (mfc) as piezoelectric actuator, J. Vibroeng. 2 (2009) 263–264.
[46] W. Niu, B. Li, T. Xin, W. Wang, Vibration active control of structure with parameter perturbation using fractional order positive position feedback controller, J. Sound Vibr. 430 (2018) 101–114.
[47] R.C. Dorf, R.H. Bishop, Modern Control Systems, Pearson, 2011.
[48] S. Kanev, T.V. Engelen, Wind turbine extreme gust control, Wind Energy 13 (2010) 18–35.